Hybrid Compartment Model Formulation for Accelerated Bolus Fitting

Diogo Filipe Silva
Chair for Medical Information Technology
RWTH Aachen University
Aachen, Germany
silva@hia.rwth-aachen.de

Steffen Leonhardt
Chair for Medical Information Technology
RWTH Aachen University
Aachen, Germany
leonhardt@hia.rwth-aachen.de

***Abstract*—Curve fitting is the central step in extracting hemodynamic parameters from various contrast-based medical imaging modalities. Yet, using functions derived from compartment modelling principles with basic nonlinear least-squares approaches is challenging and computationally expensive. This contribution describes a novel hybrid approach to efficiently and accurately estimate blood flow and volume, which was compared against the state-of-the-art via extensive realistic simulations for computerized and electrical impedance tomography, having shown superior robustness, speed, and overall accuracy.**

***Index Terms*—dynamic contrast-enhanced imaging, tracer kinetics, compartment modelling, optimization**

I. Introduction

Dynamic contrast-enhanced (DCE) medical imaging modalities are particularly useful to accurately derive spatially-resolved hemodynamic parameters, like blood flow, of a particular anatomical region, thus enabling the detection and localization of local perfusion defects, including e.g. ischemic or hemorrhagic strokes. This technology typically involves a tomographic modality, such as computerized tomography (CT), electrical impedance tomography (EIT), magnetic resonance imaging (MRI), or echocardiography (Echo), and the injection of a modality-specific substance, i.e. a tracer, intravenously in the patient. The latter produces a local enhancement of the image signal synchronous to its passage through the anatomical region.

A. Tracer Kinetics in Perfusion Imaging

The estimation of hemodynamic parameters using DCE imaging modalities is based on the principles of tracer kinetics. This refers to the mathematical interpretation of tracer transport (inflow, outflow, and/or trapping) throughout the different tissues it traverses from the its original injection locus, to the target locus, where measurements occur [1]. Fig. 1 provides an illustrative block diagram describing the tracer path along the cardiovascular system carried by flowing blood volumes. The tracer injection delivers an often assumed instantaneous impulse of concentration C_{tracer}, which is then diluted over the different volume compartments along its path, yielding a measurable time-concentration curve (TCC) C_l at different loci

This work has been funded by Deutsche Forschungsgemeinschaft (DFG) under grant no LE 817/40-1 and RE 4418/1-1.

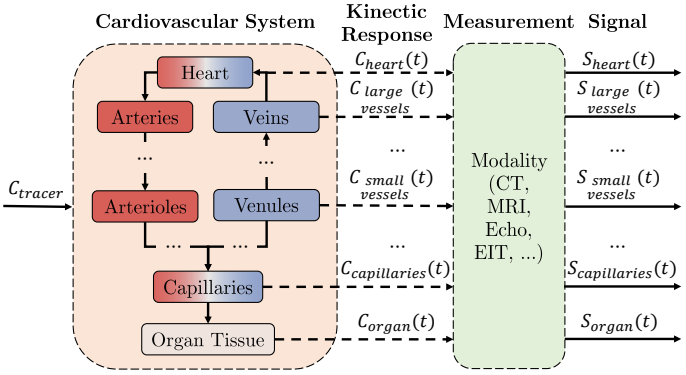

Fig. 1. An illustrative overview of tracer kinetics in medical imaging.

$l = \{heart, vessel, organ, ...\}$, traditionally accessed through invasive means, e.g., catheters [2]. Nowadays, DCE imaging allows measurement proxies of these concentrations to be obtained from pixels or voxels' time-intensity signals (TIS) S_l. A known intensity-to-concentration conversion formula exists for each modality, allowing C_l to be recovered from S_l, effectively making the latter a proxy for blood flow.

B. Connection to Compartment Modelling

Tracer kinetics are most commonly explained in the light of compartment modelling, as depicted in Fig. 2, where every organ or tissue (e.g., in Fig. 1) can be seen as n sequential ideally mixing compartments with identical volume V traversed by a constant flow Q of tracer [3]. Through the differential equations describing the conservation of mass for all n compartments, a transfer function h_n for the organ can be obtained as

$$h_n = \left(\frac{Qn}{V}\right)^n \frac{t^{n-1}}{(n-1)!} e^{-\frac{Qn}{V}t}, \tag{1}$$

which convoluted with the incoming tracer concentration C_{in} leads to the corresponding diluted concentration C_{out} [4], [5]. An ideal mass transporter (idealized vessel) can for instance be approximated with $n \to \infty$, while a reservoir with the opposite behaviour can be modelled by $n = 1$. Under the assumption of an impulse-like input C_{in}, the transfer function

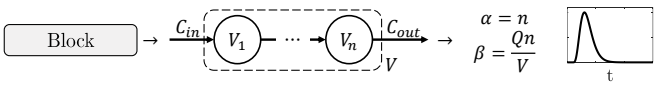

Fig. 2. Compartment model interpretation of organs or tissues, represented as blocks in Fig. 1. The volume V of a compartment is equally partitioned into n sequential compartments traversed by a constant flow Q. The gamma-variate function presented in Eq. (2), whose waveform is displayed, describes the impulse response of these systems.

h_n was found to output C_{out} morphologically identical to a gamma-variate function

$$\gamma(t|\alpha,\beta) = \beta^{\alpha}\frac{t^{\alpha-1}}{(\alpha-1)!}e^{-\beta t}, \tag{2}$$

defined by the positive shape-defining parameters α and β, connected to the parameters of the compartment formulation in Eq. (1) through $\alpha = n$ and $\beta = \frac{Qn}{V}$ [6]. It was further shown that, despite modality-induced variations in TISs measured from a single CIS, there is a unique underlying gamma-variate-shaped transfer function unequivocally identifying the hemodynamic state of the imaged region [7].

C. Extraction of Hemodynamic Parameters

Hemodynamic parameter extraction is typically performed after the proper modality-specific conversion is applied to the measured TISs to arrive at their underlying TCCs. However, since the conversion from signal intensity to tracer concentration is considered to be a linear scaling factor in our contemplated modalities DCE-EIT and DCE-CT, this step can be performed directly on the TISs if relative (and not absolute) parametrization suffices [5].

In particular, one of the most common strategies is to fit an $A_{\{C,S\}}$-scaled and t_0-delayed gamma-variate model of Eq. (2) to pixel/voxel intensity or tracer concentration data after baseline removal. A nonlinear least-squares optimization problem may be defined

$$\hat{\theta} = \underset{\theta}{\operatorname{argmin}}|| \{C,S\}_l - A_{\{C,S\}}\gamma(t-t_0|\alpha,\beta)||^2, \tag{3}$$

where four optimal parameters $\theta = [A_{\{C,S\}}, t_0, \alpha, \beta]$ need to be determined in order to arrive at regional values of blood flow Q [4]. Unfortunately, this methodology is hindered by important drawbacks. For one, the nonlinearity of the gamma-variate formulation, and the co-dependence of the shape parameters α and β introduces additional local minima to the cost function. Also, the native gamma-variate formulation does not consider the frequent recirculation effects (detailed in Chapter II-A), leading to a systematic overestimation of some hemodynamic parameters, e.g., blood flow [8]. For another, medical imaging data is typically high-dimensional in time and space, with single DCE-EIT recordings having thousands $\left(10^3\right)$ of pixels, and single DCE-CT recordings having millions $\left(10^6\right)$ of pixels, greatly elevating the computational demand of the optimization.

This work introduces a partially linear (hybrid) gamma-variate formulation extended to account for different recirculation effects, and an approach to parameterize it fast, robustly and accurately from data. Moreover, this novel method was validated against the state-of-the-art nonlinear one with DCE-EIT and DCE-CT data simulated over a wide range of hemodynamic parameter configurations.

II. Materials and Methods

Firstly, an existing multimodal tracer signal synthesizer [9] will be reintroduced in Chapter II-A, and its employment in the creation of a validation dataset for this work will be described in Chapter II-B. Ultimately, the hybrid optimization strategy to parametrize the gamma-variate extension used for the synthesizer is presented in Chapter II-C.

A. Multimodal Bolus Synthesizer

In [9], a synthesizer of DCE-CT and DCE-EIT TISs from a common underlying source TCC was presented to overcome the lack of quality ground truth to validate compartment-model-based perfusion estimation algorithms.

Given that both shape parameters β and α influence the function's maximum amplitude apart from its shape, an equivalent but alternative gamma-variate formulation with decoupled parameters will hereafter be used. Applying the variable changes $\alpha \leftarrow \alpha + 1$ and $\beta \leftarrow \frac{1}{\beta}$ to Eq. (2), we arrive at

$$\gamma(t|\alpha,\beta) = t^{\alpha}e^{\left(-\frac{t}{\beta}\right)},$$

where the time at which the peak amplitude is achieved becomes $T_{peak} = \alpha\beta$. Note that $\gamma(T_{peak}|\alpha,\beta) = T_{peak}^{\alpha}e^{\left(-\frac{T_{peak}}{\beta}\right)} = T_{peak}^{\alpha}e^{\alpha}$. It naturally follows that using only one shape parameter α suffices to describe the same function with unitary peak amplitude as

$$\gamma(t|T_{peak},\alpha) = T_{peak}^{\alpha}t^{\alpha}e^{-\alpha\left(1-\frac{t}{T_{peak}}\right)}. \tag{4}$$

The synthesizer models the so-called "first pass" of the tracer through an anatomical region l, effect A in Fig. 3, based on the decoupled gamma-variate function of Eq. (4). Specifically, as a TCC,

$$C_{F,l}(t|A_C,t_0,T_{peak},\alpha) = A_C\gamma(t-t_0|T_{peak},\alpha), \tag{5}$$

where the following user-defined hemodynamic parameters are considered: peak tracer concentration A_C, time of arrival t_0, time to peak T_{peak}, mean transit time MTT and relative dispersion RD. The latter two are used to set α according to the relations $MTT = (\alpha+1)\frac{T_{peak}}{\alpha}$ and $RD = \frac{1}{\alpha+1}$. A unique set of blood flow Q, blood volume V, and number of compartments n is, therefore, also simulated.

This synthesizer further accounts for two recirculation effects: secondary tracer passes, referred to as B in Fig. 3, and cumulative recirculation effects, represented in the same figure as C and D. The latter are characterized by a combination of the progressive detachment of tracer molecules from the moving bolus concentrate, consequently diluted over the larger intravascular volume, and the two-way transport of tracer material between the intra- and extravascular volumes through

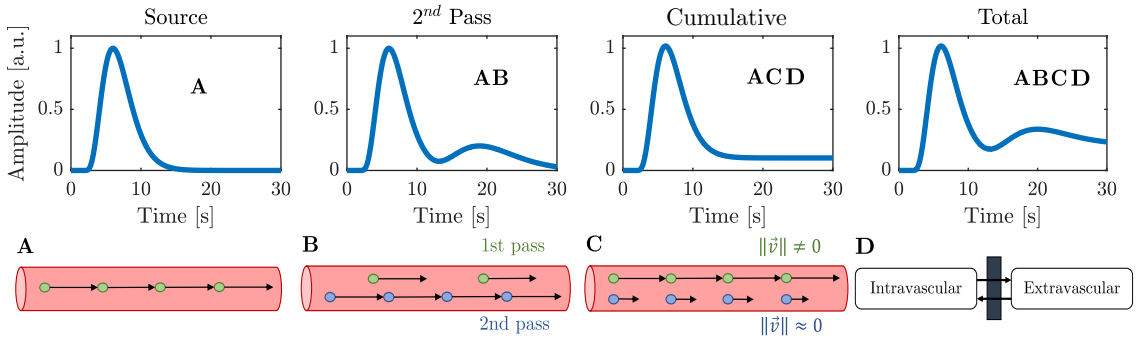

Fig. 3. Simulated curve for each effect (top), and illustrative representation of the physiological effects covered by the synthesizer (bottom). Ideal blood vessels are depicted as red cylindrical tubes, with flowing tracer molecules coloured green for the bolus first pass, and blue for the bolus second pass. A representation of the capillary membrane is also provided as a semi-permeable wall between two mutually-affecting compartments.

the capillary membranes [8]. This component was modelled as

$$C_{\Sigma,l}(t|A_C, t_0, T_{peak}, \alpha) = \int_0^t C_{F,l}(\tau)d\tau. \tag{6}$$

This is particularly relevant to distinguish signals obtained from tracer substances with different capacities to traverse the cell membrane (e.g., due to molecular size), like the more diffusible electrically conductive NaCl in EIT, and less diffusible radiodense iodine-based in CT.

The superposition of first and secondary passes can simply be modelled by the summation of P TCCs described by $C_{F,l}$ of Eq. (5) and $C_{\Sigma,l}$ of Eq. (6), yielding

$$\begin{aligned} &C_{T,l}(t|\mathbf{A_C}, \mathbf{t_0}, \mathbf{T_{peak}}, \boldsymbol{\alpha}, \mathbf{RF}, P) = \\ &\sum_{p=1}^{P}(1 - RF_p) \cdot C_{F,l,p}(t) + RF_p \cdot C_{\Sigma,l,p}(t), \end{aligned} \tag{7}$$

where $\mathbf{A_C}, \mathbf{t_0}, \mathbf{T_{peak}}, \boldsymbol{\alpha}$ and $\mathbf{RF}$ are now P-element vectors whose rows are descriptive of a single pass p. The recirculation factors $RF \in [0, 1]$ are the tracer fraction retained in cumulative recirculation effects. Reciprocally, $(1 - RF)$ is the tracer fraction flowing intravascularly aggregated to the moving tracer bolus in compliance with conservation of mass.

Finally, K-long vectors of modality-specific TISs $\mathbf{s_l} \in \mathbb{R}^{K\times 1}$ for each of the modelled components can be achieved with an additional modality-specific scaling factor A_S, respective to a linear concentration-to-intensity conversion, and a fixed sampling-rate, finalizing the synthesizer formulation

$$\mathbf{s_{m,l}}(k) = A_S C_{m,l}(kT), \tag{8}$$

where $m = \{F, \Sigma, T\}$ labels the desired effect, $k = 1, \ldots, K$ denote the samples, and T the modality's sampling period.

B. Validation Dataset

A total of two validation datasets - one for each of the two modalities - were obtained through a grid-sweep approach, in which physiological bounds were defined for each simulation parameter, as seen in Table I, and a finite number of possible parameter combinations were sampled from the model. All effects depicted in Fig. 3 were included in the simulated TISs, amounting to the formulation in Eq. 8 with $m = T$. The second pass parameters were obtained from first pass ones by scalar modifiers - also specified in Table I. Each TIS was made 60 s long, with DCE-CT signals being sampled at 1 Hz, and DCE-EIT signals at 50 Hz. In total, an average of $2.592 \cdot 10^5$ TISs were successfully simulated per dataset. All tests were run on a machine boasting an Intel® Core™ i5-9500 CPU @ 3.00 GHz.

C. Accelerated Hybrid Formulation

As in the nonlinear approach of Eq. (3), the removal of the signal's baseline is the first step. Foremost, $\mathbf{k_0}$, the samples corresponding to the onset (t_0) of each tracer pass $\mathbf{s_{F,l}}$, and $\mathbf{K_{peak}}$, the samples at which they are maximized, must be obtained via signal processing to enable the partial linearization of the total model [10]. Since these parameter vectors are maintained constant, they will be omitted from further mentions to $\mathbf{s_{m,l}}(k), m = \{F, \Sigma, T\}$ and $\mathbf{s_{\Sigma,l}}(k)$ will be considered independent from them. The discrete equivalent of the time normalization $t'_p = \frac{t - t_{0,p}}{T_{peak,p} - t_{0,p}}$ is then applied to Eq. 8, leading to $k'_p = \frac{k - k_{0,p}}{K_{peak,p} - k_{0,p}}$, and yielding its discrete expansion in matrix form,

$$\begin{aligned} &\mathbf{s_{T,l}}(k) = \\ &\sum_{p=1}^{P} A_p \left((1 - RF_p)\mathbf{s_{F,l,p}}(k'_p|\alpha_p) + RF_p \mathbf{s_{\Sigma,l,p}}(k'_p|\alpha_p)\right) = \\ &\begin{bmatrix} \mathbf{s_{\Sigma,l,1}}(k'_1|\alpha_1) - \mathbf{s_{F,l,1}}(k'_1|\alpha_1) \\ \mathbf{s_{F,l,1}}(k'_1|\alpha_1) \\ \vdots \\ \mathbf{s_{\Sigma,l,P}}(k'_P|\alpha_P) - \mathbf{s_{F,l,P}}(k'_P|\alpha_P) \\ \mathbf{s_{F,l,P}}(k'_P|\alpha_P) \end{bmatrix}^T \begin{bmatrix} A_1 RF_1 \\ A_1 \\ \vdots \\ A_P RF_P \\ A_P \end{bmatrix} = \mathbf{X}\boldsymbol{\theta}, \end{aligned} \tag{9}$$

where $A_p = A_{C,p} A_{S,p}$. The total number of linear parameters grows by $2P$, and nonlinear parameters by P, resulting in $\mathbf{X} \in \mathbb{R}^{K\times 2P}$ and $\boldsymbol{\theta} \in \mathbb{R}^{2P\times 1}$. Given a measured TCC or TIS

TABLE I

GRID OF PHYSIOLOGICAL PARAMETERS AND SCALING FACTORS SWEPT IN ORDER TO CREATE THE CT AND EIT DATASETS.

Tracer Pass		A	$\mathbf{T_{peak}}$	MTT	RD	RF
1st (params.)	min.	0.25	1.00	1.00	0.10	0.05
	step	3	4	8	3	4
	max.	1.75	7.00	8.00	0.30	0.30
2nd (factors)	min.	0.10	0.50	1.10	1.10	1.10
	step	3	5	5	3	1
	max.	0.50	3.00	1.20	1.15	1.10

*Units: **A** [n.u.], $\mathbf{T_{peak}}$ [s], **MTT** [s], **RD** [a.u.], **RF** [n.u.]

signal $\mathbf{y} \in \mathbb{R}^{K\times 1}$, only the parameter $\boldsymbol{\alpha}$ must be obtained nonlinearly through

$$\hat{\boldsymbol{\alpha}} = \underset{\boldsymbol{\alpha}}{\operatorname{argmin}} f(\mathbf{A}, \boldsymbol{\alpha}, \mathbf{RF}),$$

with $f(\mathbf{A}, \boldsymbol{\alpha}, \mathbf{RF}) = ||\mathbf{y} - \mathbf{s_{T,l}}(\mathbf{A}, \boldsymbol{\alpha}, \mathbf{RF})||^2$ being the loss function, while the remaining ones **A** and **RF** might be obtained in the linear least-squares sense $\hat{\boldsymbol{\theta}} = (\mathbf{X}^T\mathbf{X})^{-1}\mathbf{X}^T\mathbf{y}$. Algorithm 1 describes an optimization approach to determine $\boldsymbol{\alpha}$ and $\boldsymbol{\theta}$ with alternating gradient-based and ordinary least-squares (OLS) updates.

Algorithm 1 Hybrid fitting optimization.

$tol \leftarrow 10^{-3}$
$\eta \leftarrow 10^{-1}$
$k'_p \leftarrow \frac{k-k_{0,p}}{K_{max,p}-k_{0,p}}$
$\boldsymbol{\alpha_0} \leftarrow \begin{bmatrix} 5 & \dots & 5 \end{bmatrix}$
$\mathbf{X_0} \leftarrow \begin{bmatrix} \mathbf{s_{\Sigma,l,1}}(\alpha_{0,1}) - \mathbf{s_{F,1,l}}(\alpha_{0,1}) & \mathbf{s_{F,1,l}}(\alpha_{0,1}) & \dots \end{bmatrix}$
$\hat{\boldsymbol{\theta}} \leftarrow (\mathbf{X_0}^T\mathbf{X_0})^{-1}\mathbf{X_0}^T\mathbf{y}$
$f_0 \leftarrow ||\mathbf{y} - \hat{\mathbf{X}}_\mathbf{0}\hat{\theta}||^2$
while $f_i > tol$ **do**
  $\hat{\boldsymbol{\alpha}}_\boldsymbol{i} = \hat{\boldsymbol{\alpha}}_{\boldsymbol{i-1}} + \eta\frac{\partial f}{\partial \boldsymbol{\alpha_{i-1}}}$ ▷ gradient-based update
  $\hat{\mathbf{X}}_\mathbf{i} \leftarrow \begin{bmatrix} \mathbf{s_\Sigma}(\hat{\alpha}_{i,1}) - \mathbf{s_F}(\hat{\alpha}_{i,1}) & \mathbf{s_F}(\hat{\alpha}_{i,1}) & \dots \end{bmatrix}$
  $\hat{\boldsymbol{\theta}} \leftarrow (\hat{\mathbf{X}}_\mathbf{i}^T\hat{\mathbf{X}}_\mathbf{i})^{-1}\hat{\mathbf{X}}_\mathbf{i}^T\mathbf{y}$ ▷ OLS update
  $f_i \leftarrow ||\mathbf{y} - \hat{\mathbf{X}}_\mathbf{i}\hat{\theta}||^2$
end while
$\hat{A}_p \leftarrow \hat{\boldsymbol{\theta}}_{2p,1}$
$\hat{RF}_p \leftarrow \frac{\hat{\boldsymbol{\theta}}_{2(p-1)+1,1}}{\hat{A}_p}$

III. RESULTS AND DISCUSSION

For comparable results with the proposed hybrid approach of Eq. (9) and Algorithm 1, the nonlinear method in Eq. (3) was extended with the cumulative recirculation component in Eq. (7). Ground truth values for blood flow and volume were firstly obtained from the simulated TISs: with the Stewart-Hamilton equation, where blood flow (hBF) is the inverse of the first pass' area under the curve; with Fick's principle, where blood flow (fBF) is the first pass' maximum slope before T_{peak} [11]. Finally, the respective blood volumes were obtained according to the central volume theorem as $\{h,f\}BV = \{h,f\}BF \cdot MTT$ [5]. The relative error between the estimated and ground truth parameters were calculated along with the overall curve fitting RMSE, and the computation time (summarized in Fig. 4).

Given the comprehensiveness of the validation dataset, which contains several thousands of realistic parameter configurations and an equally high number of edge cases, we believe that the results are a good global representation of the performance of both algorithms. To enable similar large analyses in the future in the field of CT and/or EIT, the

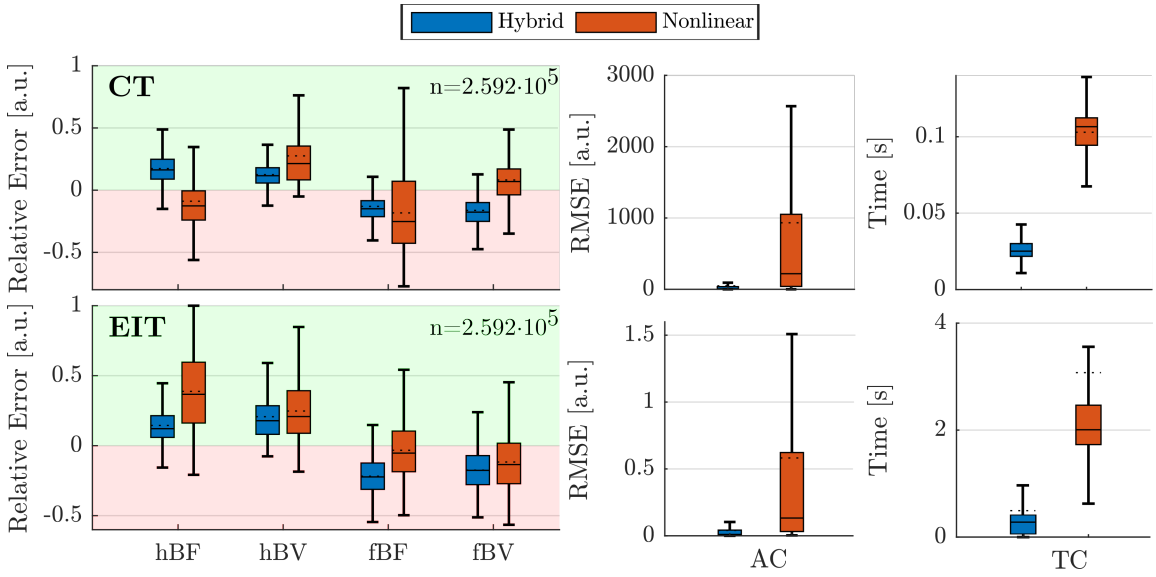

Fig. 4. Validation results for the nonlinear and the proposed hybrid approaches applied to the simulated CT (top row), and EIT (bottom row) datasets. Blood flow and volume according to Stewart-Hamilton's equation and Fick's principle were used for comparison along with the fitting RMSE (AC) and computational time (TC) in the form of box plots. The hybrid approach seems to be able to estimate the hemodynamic parameters accurately and more robustly, while providing a closer reconstruction, and a greatly reduced computation time.

synthesizer code was made freely available in the GitHub repository: CT-EIT-BolusGenerator. Fig. 4 shows that the hybrid approach displays similar median error values to the state-of-the-art but with smaller dispersion. Surprisingly, this is also the case for the overall RMSE and the computational time, hinting at a higher robustness of the hybrid approach, which might be related to the decoupling of the shape parameters of the used gamma-variate formulation, as well as the simplification of the optimization problem by reducing the number of nonlinear terms. In general, both approaches seem to over- and underestimate the hemodynamic parameters similarly - Stewart-Hamilton-derived metrics tend to be overestimated, while Fick's principle ones tend to be underestimated. An acceleration of almost 10X seems to be attainable with the hybrid method. This confirms what is theoretically expected, given that the number of nonlinear parameters is $5P$ for the state-of-the-art approach, with P being the number of passes to be fitted. These findings seem to strongly support the use of the proposed approach for both modalities as the computational burden is greatly reduced without estimation accuracy penalties. A demo of the proposed approach with a more sophisticated second-order gradient-based update (trust-region reflective algorithm) can be found in the GitHub repo along with sampled data from the model: CT-EIT-HybridFit.

IV. Conclusion

This contribution extensively describes a hybrid approach to hemodynamic parameter estimation for contrast-based imaging data. A realistic signal synthesizer was employed to produce a extensive validation datasets to compare the proposed approach to the state-of-the-art one. The hybrid method was shown to be superior by maintaining the estimation accuracy of individual parameters, improving the overall reconstruction error, robustness, and computation time, making it a reliable alternative for applications with restricted processing power. Notwithstanding, future work is still necessary to better characterize the algorithms strengths and weaknesses before it can be launched into the processing workflow in clinical domain. For instance, a more targeted analysis of performance on certain parameter configurations, as well as comparisons with further relevant algorithms (e.g., fully linear approaches) would be of great pertinence.

References

[1] T. S. Koh, S. Bisdas, D. M. Koh, and C. H. Thng, "Fundamentals of tracer kinetics for dynamic contrast-enhanced MRI," J. Magn. Reson. Imaging, vol. 34, no. 6, pp. 1262–1276, Dec. 2011.

[2] K. Zierler, "Indicator Dilution Methods for Measuring Blood Flow, Volume, and Other Properties of Biological Systems: A Brief History and Memoir," Ann. Biomed. Eng., vol. 28, no. 8, pp. 836–848, Aug. 2000.

[3] C. Cobelli, D. Foster, and G. Toffolo, Tracer Kinetics in Biomedical Research. Boston, MA: Springer US, 2002.

[4] B. Hentze et al., "A model-based source separation algorithm for lung perfusion imaging using electrical impedance tomography," Physiol. Meas., vol. 42, no. 8, p. 084001, Aug. 2021.

[5] A. Fieselmann, M. Kowarschik, A. Ganguly, J. Hornegger, and R. Fahrig, "Deconvolution-Based CT and MR Brain Perfusion Measurement: Theoretical Model Revisited and Practical Implementation Details", Int J Biomed Imaging. 2011; 2011:467563.

[6] H. K. Thompson, C. F. Starmer, R. E. Whalen, and H. D. Mcintosh, "Indicator Transit Time Considered as a Gamma Variate," Circ. Res., vol. 14, no. 6, pp. 502–515, Jun. 1964.

[7] P. Meier and K. L. Zierler, "On the Theory of the Indicator-Dilution Method for Measurement of Blood Flow and Volume," J. Appl. Physiol., vol. 6, no. 12, pp. 731–744, Jun. 1954.

[8] V. Patil and G. Johnson, "An improved model for describing the contrast bolus in perfusion MRI," Medical Physics, vol. 38, no. 12, pp. 6380–6383, Nov. 2011.

[9] D. F. Silva, S. Leonhardt, and C. Ngo, "A Top-to-Bottom Generator of EIT and CT Bolus Signals," in International Conference on Bioelectromagnetism, Electrical Bioimpedance, and Electrical Impedance Tomography, Kyung Hee University, Seoul, Korea, 2022, pp. 70–73.

[10] F. Schuderer, M. Kircher, O. Dössel, B. Stender, T. Bluth, and M. Gama de Abreu, "Introducing a Linear Gamma Variate Fit to Measure Pulmonary Perfusion with Electrical Impedance Tomography," Curr. Dir. Biomed. Eng., vol. 6, no. 3, pp. 345–348, Sep. 2020.

[11] E. T. Gilbert-Kawai and M. D. Wittenberg, "Stewart–Hamilton equation," in Essential Equations for Anaesthesia, Cambridge University Press, 2014, pp. 92–107.